THE ISOCAM DETECTORS: AN OVERVIEW

O. BOULADE AND P. GALLAIS
*Service d'Astrophysique, DAPNIA, CEA/Saclay**
91191 Gif sur Yvette Cedex FRANCE

Abstract. The two detectors of the ISOCAM camera on board the ISO spacecraft have performed nominally for the entire duration of the mission. Their main properties (dark current, noise and responsivity) stayed very stable from the first tests on ground to the end of the life of ISO, a 6 years long period. The main limitation to the sensitivity of the observations came from transients in the signal delivered by the detectors, induced either by a change in the sources fluxes or by glitches.

1. Introduction

The ISOCAM camera [1] on board the ISO Infrared Space Observatory [2] had two detectors (see figure 1): the short wave (SW) detector used a InSb substrate and a Charge Injection Device readout method, for wavelengths from 2.5 to 5 microns, while the long wave (LW) detector used a Si:Ga substrate with a Direct Readout Output circuit, for wavelengths from 4 to 17 microns. Both detectors had 32x32 100μx100μ pixels. A good introduction to the main characteristics of these detectors can be found in the ISOCAM Observer's Manual [3].

The SW detector was developed by Société Anonyme de Télécommunications and Département de Recherche Spatiale at Observatoire de Paris-Meudon. The readout noise of this detector was about 700 e^-, at an operating temperature of about 5.5K.

The LW detector was developed by two departments of Commissariat à l'Energie Atomique: LETI/LIR Laboratoire Infra-Rouge and Service d'Astrophysique. The readout noise of this detector was about 180 e^-, and its operating temperature was regulated at 3.8K.

*oboulade@cea.fr, pgallais@cea.fr

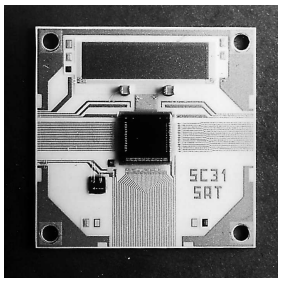

SW 2.5-5µ
32x32 100µx100µ
InSb CID
SAT/DESPA
R.N. 700 e⁻
T~5.5K

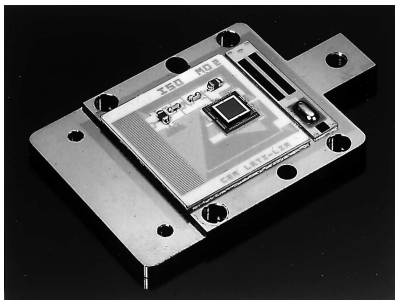

LW 4-17µ
32x32 100µx100µ
Si:Ga DRO
LETI-LIR/SAp
R.N. 180 e⁻
T=3.8K

Figure 1. The ISOCAM detectors

This paper will focus on the following characteristics: dark current and noise, long term stability of the responsivity, LW saturation. A number of more specific papers are presented elsewhere in these proceedings: LW transient modeling [4], SW transient modeling [5], LW dark current subtraction [6], photometry [7], radiation effects [8], effects and correction of glitches [9] and LW ultimate sensitivity [10].

For both detectors, the ISOCAM team designed a set of calibrations (flat field measurements at two wavelengths using the ISOCAM internal calibration sources, as well as dark current measurements at different integration times) that were executed at every revolution of the ISO spacecraft, during the so-called "deactivation" and "hand-over" windows. These measurements proved to be very useful to study the long term behavior of the detectors during the ISO mission and are the basis of this paper. The other main source of measurements came from the tests done on ground, during the ground calibration campaigns as well as during the integration of the instrument inside the spacecraft (the "Integrated System Tests" – IST).

2. Dark current and noise

2.1. SW DETECTOR

Figure 2 shows the dark current level and noise in the dark current images of the SW detector, for the 6 seconds integration time, for the whole ISO mission. The dark current level and noise just after launch were the same

as during the ground tests, and stayed very stable for the whole duration of the mission, with the exception of a small increase (about 2.5%) of the noise after revolution 700.

The bottom curve of figure 2 shows the E1 channel of NOAA's geosynchronous GOES-9 spacecraft, which is sensitive to trapped electrons in the outer zones of the Van Allen belts. The spikes seen in both the SW detector signal and noise curves are clearly correlated with the variations of the electron fluence in the radiation belts (see section 2.3).

2.2. LW DETECTOR

The dark current level and noise of the LW detector, at 2 seconds integration time, are plotted in figure 3 for the whole ISO mission. The dark current level at the beginning of the mission was the same as during the ground tests. As for the SW detector, there is a very good correlation of the spikes seen in both the signal and noise curves and the variations of the electron fluence as measured by the GOES-9 spacecraft.

We observed a slow decrease of the dark current level with time, as is best seen in figure 4 which shows the trend of the mean LW dark current level, again for the 2 seconds integration time, but measured during the "hand-over windows" (note that there are no spikes in this figure: the "hand-over window" was a period of the spacecraft orbit that was much cleaner than the "deactivation window" in terms of pollution by glitches, which confirms that the radiation belts were the cause of the spikes in the deactivation measurements).

The reset level of the LW detector (figure 5) showed in several occurrences a very strong decrease followed by a slow recovery to the normal level. There is no explanation for the time being. This was not a problem since the real images of the LW detector are built by subtraction of the reset image from the end-of-integration image, and the drop of signal is cancelled out in this operation.

Besides the mean level of the dark current, the pattern of the dark images (see figure 6) also changed, both along a given orbit and from one orbit to the next. Not taking these variations into account during the dark current subtraction step of the data processing would then generate a residual pattern at the 1-2 ADU level, which is much too high for the detection of very faint sources. A model is now available that corrects for all variations of the dark current (long trend decrease of the mean level, as well as variability of the pattern) for all integration times (see reference [6] for more details).

2.3. DARK CURRENTS AND SPACE WEATHER

As explained in the previous sections, there is a clear correlation between the dark currents of both detectors, measured in the deactivation window of the ISO spacecraft revolutions, and the electron fluxes from the radiation belts. A detailed study of this correlation is not straightforward: first, the locations of the GOES and ISO spacecrafts are not the same, although the altitude of the ISO spacecraft at the time of the deactivation measurements was always about 30000km; and second, the GOES-9 measurements used in this paper are integrated over a 24 hour period.

The effect of the proximity of the radiation belts on the two detectors was clearly to increase the mean level and the noise in the images; still, the images do not show more glitches than normal images, as if the additional signal was constant over the whole surface of the detectors. One possible explanation is that the secondary electrons produced by the interaction of the primary electrons coming from the radiation belts and the different shieldings (spacecraft shielding as well as detector block shielding) create a uniform "illumination" of the detectors. The "excess signal" for the LW detector (defined as the dark current level for a given revolution minus a "baseline" dark current level) is plotted as a function of the SW "excess signal" in figure 7.

Clearly, more work is needed to refine the analysis of these correlations: first we must take into account the precise location of the ISO spacecraft during the deactivation windows, and use only the GOES measurements done at the time of the deactivation windows. Then, the relationship between the SW and LW "excess signals" will be used to check the models of the interaction of the electrons trapped in the radiation belts with the spacecraft and the detector blocks.

3. Responsivity

3.1. SW DETECTOR

The long term behavior of the SW detector responsivity was derived first from the measurements done at the different steps of the integration of the camera in the spacecraft. The signal levels of a subset of the IST tests are plotted as a function of time (figure 8), the last point in the figure being the "checkout revolution", which, for ISOCAM, took place 7 days after launch. The levels measured (including the checkout tests) have stayed to within $\pm 2\%$ of the mean ground levels for almost 4 years.

Figure 9 shows the mean level for one of the flat field measurements done at the end of each revolution. The bimodal distribution of the signal (bottom curve) probably comes from a poor reproducibility of the position

of one or more of the wheels of the SW channel (see [11] for a detailed explanation of this behavior). There is no measurable variation of the signal delivered by the SW detector with time, for the whole mission.

3.2. LW DETECTOR

As in the previous section, figure 10 shows the signal levels of the LW detector for a subset of the IST tests as a function of time. The levels measured on ground have stayed to within $\pm 2.5\%$ of the mean ground levels for almost 4 years. As can be seen from figure 10, the levels obtained during the checkout of the instrument on revolution 7 were systematically above the nominal values by on average 24%.

At the end of the checkout revolution, we re-did some of the tests for confirmation. Figure 11 shows that the over-responsivity of the LW detector decreased with time. Given that the checkout occurred after 7 days in space, this behavior probably indicates that the LW detector trapped charges before the switch-on, with the excess charges being swept away at each readout.

Figure 12 shows the mean level for one of the flat field measurements done at the end of each revolution. There is a slight decrease of the mean level with time (about 5% after 800 revolutions). Given that the sensitivity measurements derived from the photometry of standard stars did not show such a decrease [7], the effect seen on figure 12 may well come from the internal calibration source itself.

4. Saturation

The saturation of the LW detector was one of the main problems, because of the transients induced after each such occurrence (see figure 13 for a gallery of such saturations). We could not find a satisfying way of recovering from such an event: as explained in [4], the effect of a strong flux falling on a given pixel (induced by a glitch or photons) is to decrease the responsivity of this pixel, and it can take hours or even days in extreme cases for the saturated pixel to recover its nominal responsivity.

The recovery procedure adapted by the ISOCAM team was, after a saturation had been detected in real time, to flood the whole detector array with infrared photons up to the saturation level, using the internal calibration source. Since the illumination was uniform, this had the advantage of removing the saturation pattern (i.e the remnant image of the saturating source) that would otherwise have stayed on many subsequent observations, but with the drawback that, after the procedure had been applied, all pixels were saturated and had their responsivity changed, therefore giving an inacurrate photometry.

However, this procedure was difficult to apply: first, it had to be applied within the saturating observation time slot (it was obviously not allowed to use this procedure in a subsequent non saturating observation done for a different observer...), which was not always possible given the time needed for the execution of the procedure; and second, it could not be applied within a raster observation, which was the main observing mode of the camera (applying the procedure e.g on the first raster point of an observation because of a bright star in the upper left corner of the field would then kill the entire observation...).

Therefore the best solution was to flag the possible saturations before they happen, by screening *all* ISO scheduled observations and checking the scheduled camera observing modes against the expected fluxes of *all* objects in the field of the view of the camera, be it in prime mode (when the camera was the prime observing instrument of ISO) or in parallel mode (when one of the three other instruments was prime). In the case of a conflict between the expected fluxes and the sensitivity of the scheduled observing mode, the camera was reconfigured to a less sensitive mode prior to the beginning of the observation.

5. Ultimate sensitivity

The main two limits to the sensitivity of the ISOCAM observations were the glitches induced by cosmic rays (because of the changes in pixel responsivities) and the transients in the signal levels (because of changes in the incident flux of photons). Separate papers in this volume address these problems ([9], [4]). To cope with these limitations, specific observing procedures were designed for the observations of very faint sources, which allowed these observations to reach detection limits (1σ in 1 hour) as low as 15μJy at 6.75μ and 40μJy at 15μ (see [10] for details).

6. Conclusion

The ISOCAM detectors have performed nominally for the entire life of ISO, without any significant degradation. Both the dark currents and the responsivities remained stable. The main limit on the performances came from the transients associated with glitches and changes in source fluxes. Some strange behaviors have been observed (increase in the noise of the SW dark current, drops of the LW detector reset level, distribution of the internal flat field levels of the SW detector) and are still not fully understood. Last, the effect of the radiation belts on these detectors needs a more thorough investigation, which will be very useful for studies on the shielding of detectors for future space missions.

References

1. C. Cesarsky et al.,1996, Astronomy and Astrophysics **315**, L32
2. M. Kessler et al., 1996, Astronomy and Astrophysics **315**, L27
3. The ISOCAM Team and A. Heske, 1995, http://isowww.estec.esa.nl/manuals/iso_cam/
4. A. Abergel, this volume
5. D. Rouan and D. Tiphène, this volume
6. A. Biviano et al., this volume
7. J. Blommaert, this volume
8. H. Dzitko, this volume
9. A. Claret, this volume
10. B. Altieri et al., this volume
11. P. Gallais and O. Boulade, "Report on the trend analysis of the CAM daily calibration measurements", internal report, CEA-SAp, 1998

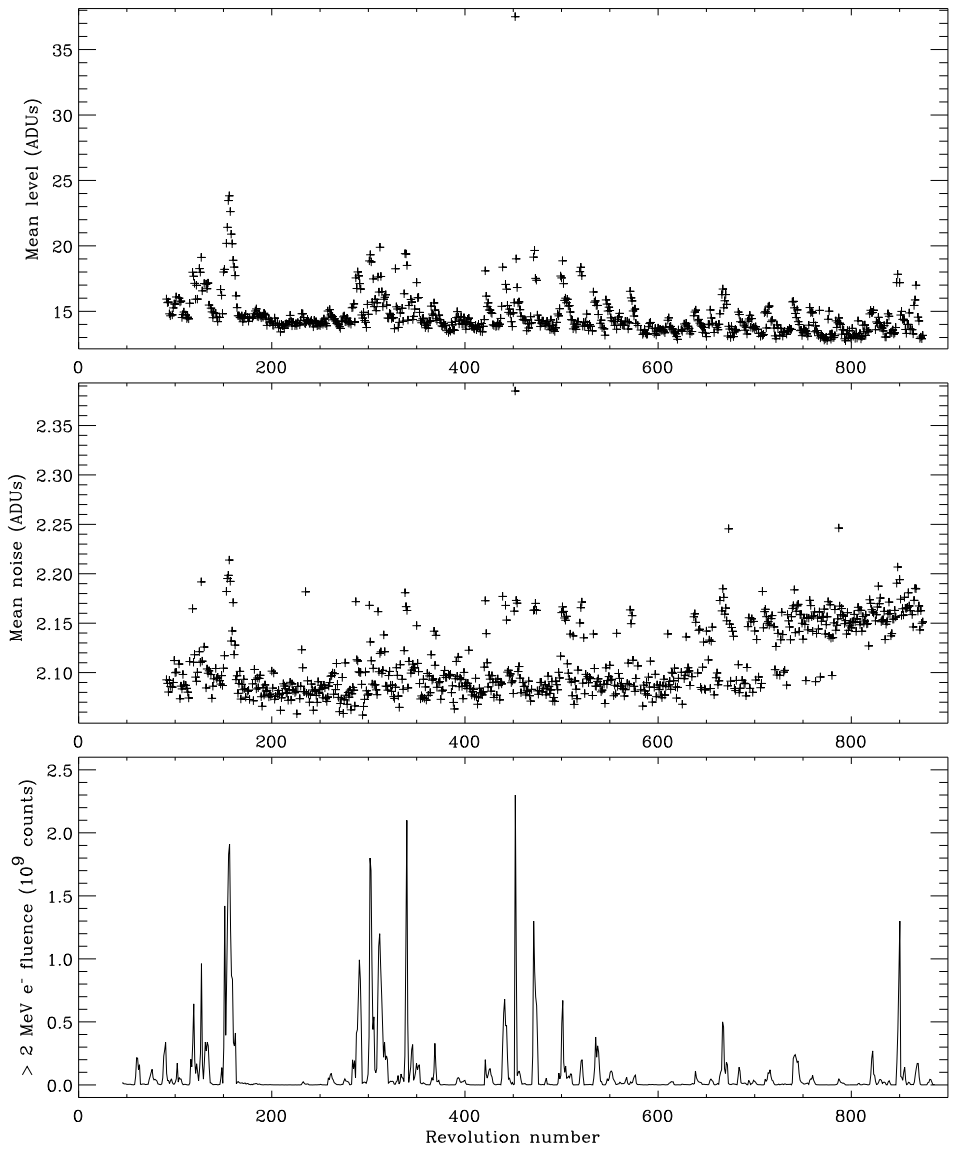

Figure 2. Long term behavior of the SW detector dark current and noise (deactivation measurements)

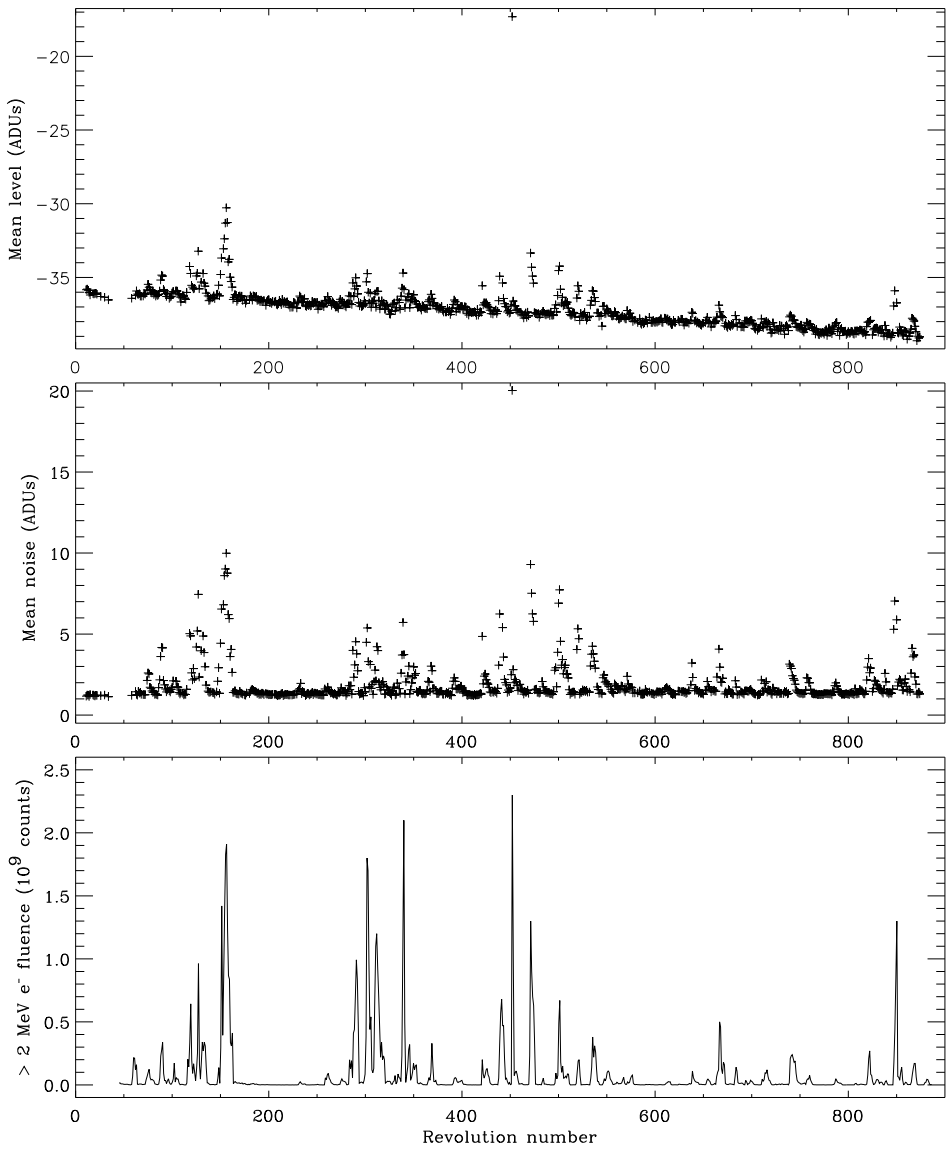

Figure 3. Long term behavior of the LW detector dark current and noise (deactivation measurements)

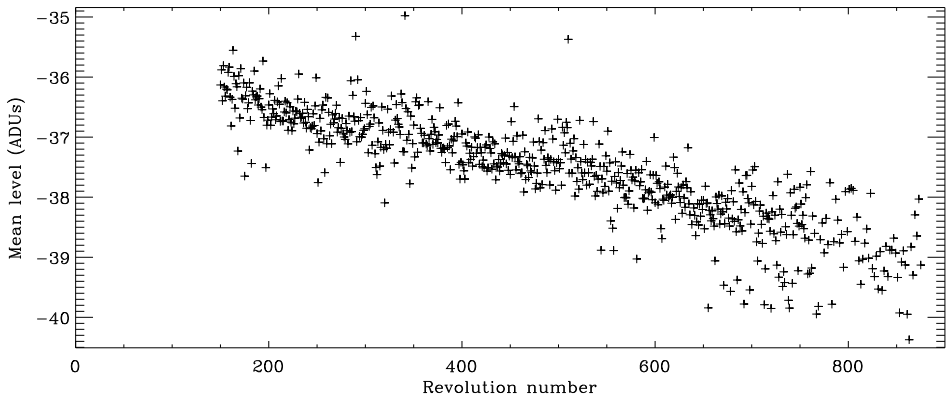

Figure 4. Long term behavior of the LW detector dark current (hand-over measurements)

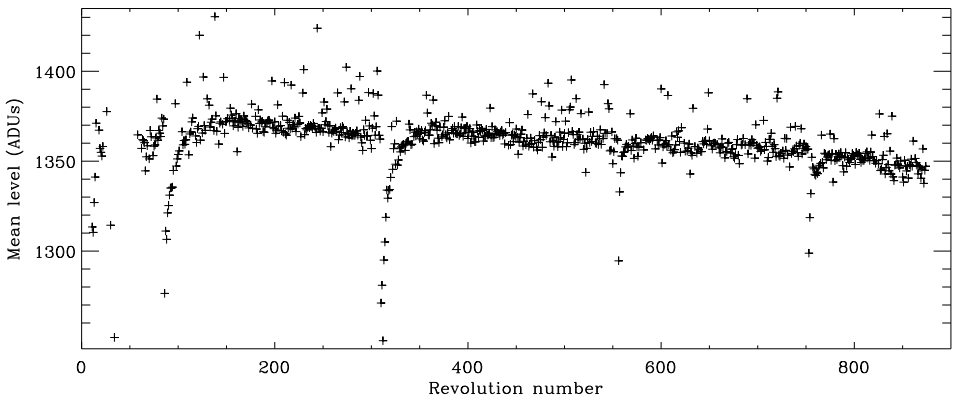

Figure 5. Long term behavior of the LW detector reset level (deactivation measurements)

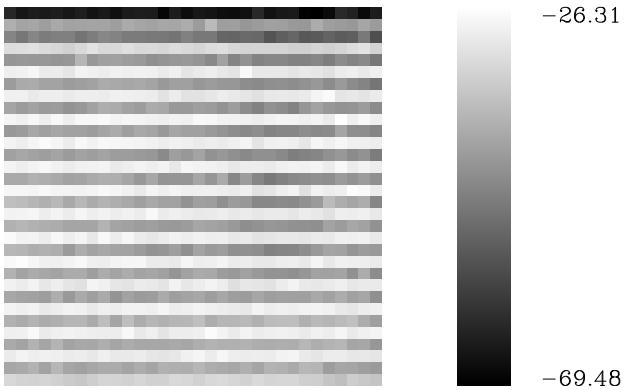

Figure 6. The LW detector dark current at 2 seconds integration time

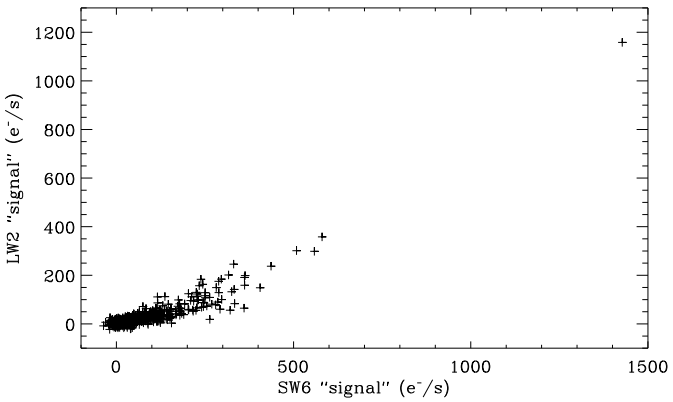

Figure 7. LW counts versus SW counts (deactivation dark measurements)

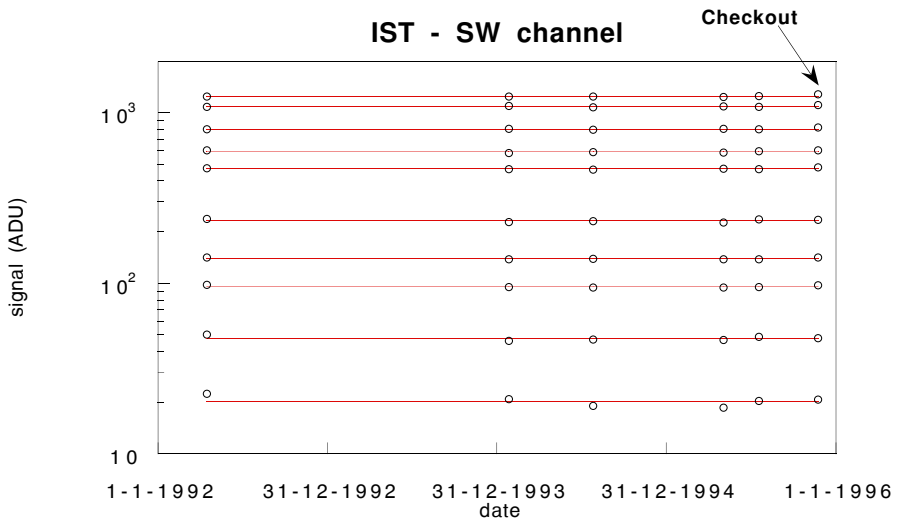

Figure 8. Trend of the SW detector levels up to launch

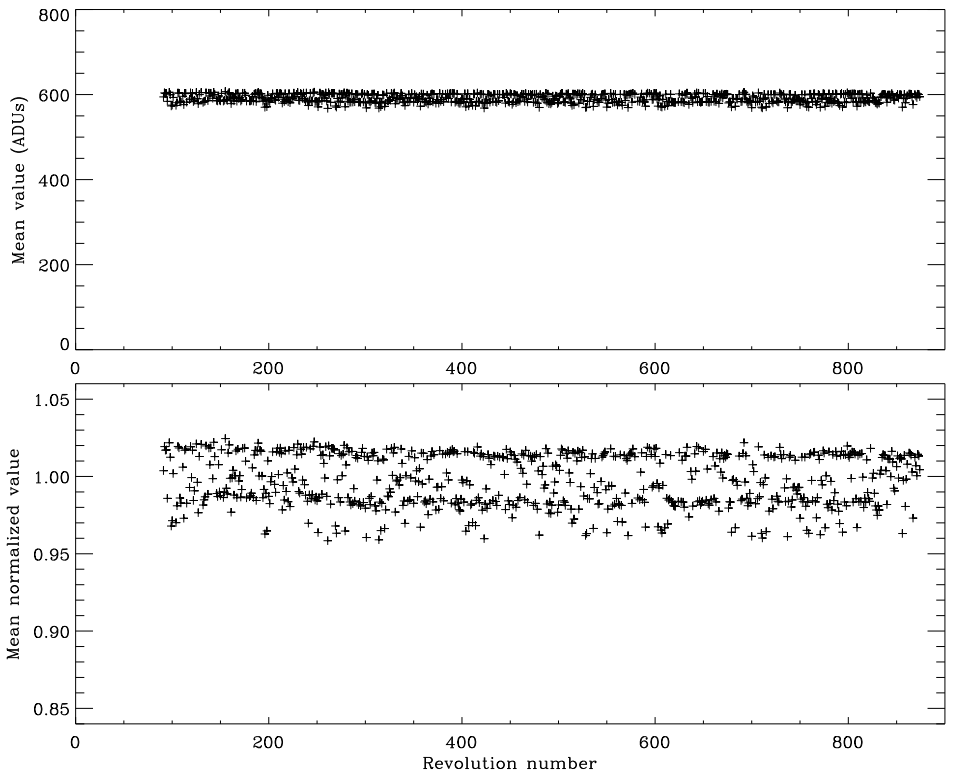

Figure 9. SW internal flat-fields during the ISO mission (deactivation measurements)

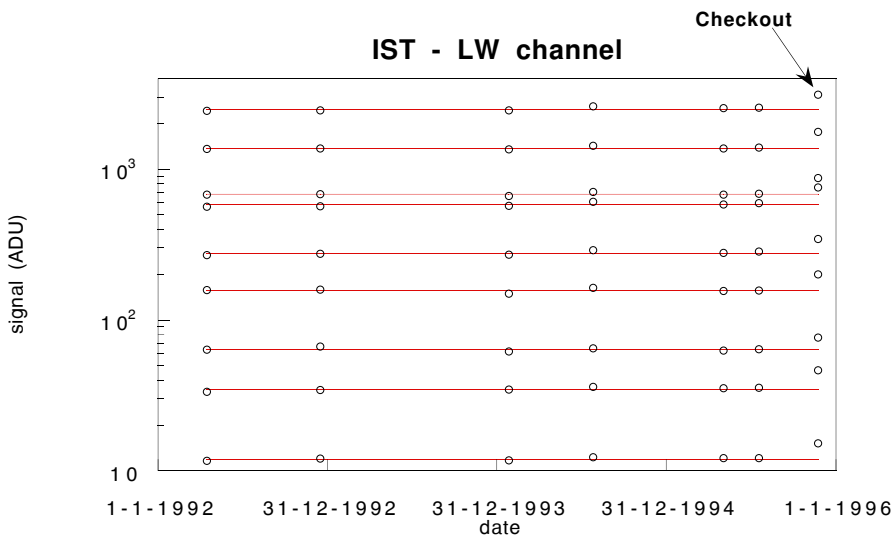

Figure 10. Trend of the LW detector levels up to launch

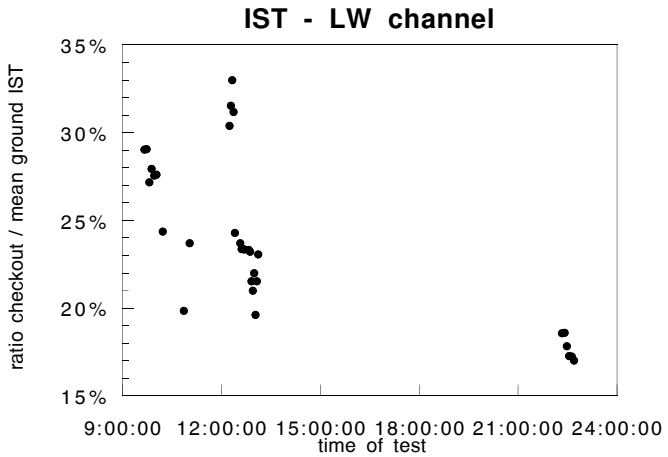

Figure 11. The LW responsivity as a function of time during checkout

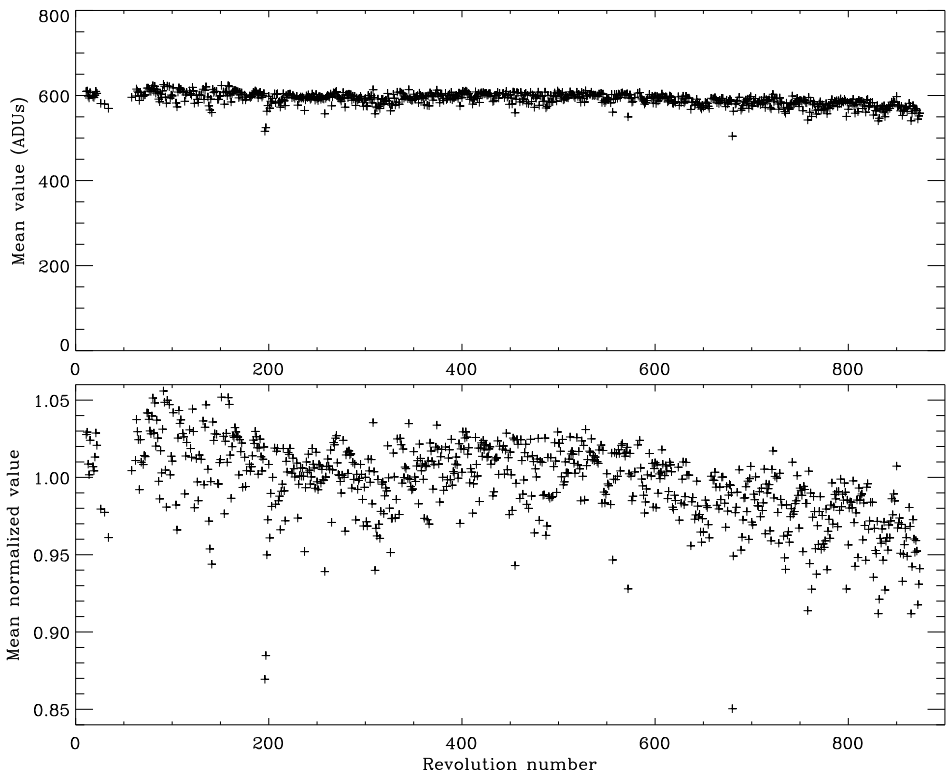

Figure 12. LW internal flat-fields during the ISO mission (deactivation measurements)

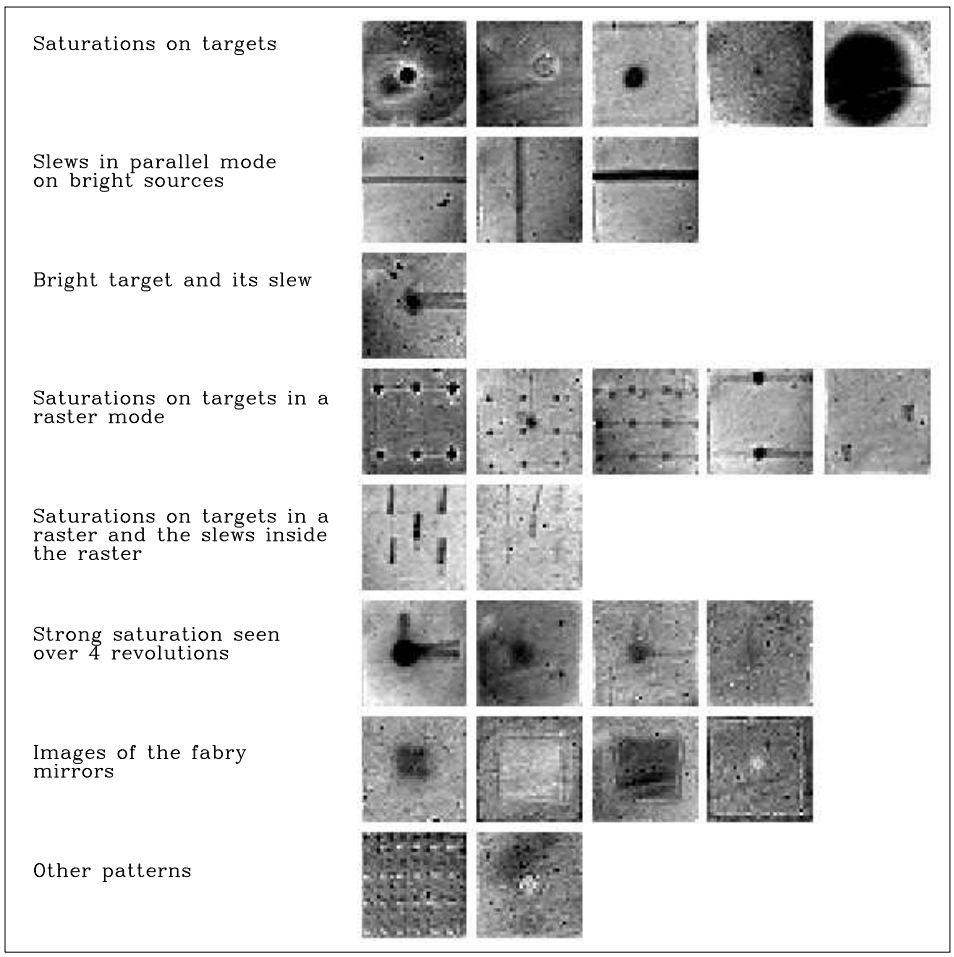

Figure 13. Some examples of saturation of the LW detector